Multiscale dynamics of pretransitional fluctuations in the isotropic phase of a lyotropic liquid crystal

C. E. Bertrand,[1,2] K. L. Linegar,[1] A. F. Kostko,[3,4] and M. A. Anisimov[1,2,*]
[1]*Department of Chemical and Biomolecular Engineering and Institute for Physical Science and Technology, University of Maryland, College Park, Maryland 20742, USA*
[2]*Department of Chemical Engineering, The Petroleum Institute, Abu Dhabi, P.O. Box 2533, United Arab Emirates*
[3]*Department of Physics, St. Petersburg State University of Refrigeration and Food Engineering, St. Petersburg 191002, Russia*
[4]*Department of Chemical and Life Science Engineering, Virginia Commonwealth University, Richmond, Virginia 23284, USA*
(Received 23 July 2008; revised manuscript received 18 December 2008; published 29 April 2009)

Using an improved static and dynamic light-scattering technique, we have observed multiscale relaxation of the pretransitional fluctuations in the isotropic phase of a cromolyn aqueous solution, a lyotropic liquid crystal where rods are formed by aggregates of disklike molecules. We have detected the onset of cromolyn aggregation about 12 °C above the transition temperature. The onset is manifested by the emergence of strong scattering due to the fluctuations of local anisotropy and by the split of the diffusion dynamics into two distinctly different modes, one associated with the relatively fast diffusion of monomer-size particles and the other one with the much slower diffusion of the cromolyn aggregates. A third observed dynamic mode is associated with the pretransitional slowing down of fluctuations of the local anisotropy. This mode behaves differently in polarized and depolarized light scattering, due to a coupling between fluctuations of the local-anisotropy and velocity fluctuations.

DOI: 10.1103/PhysRevE.79.041704 PACS number(s): 61.30.St, 81.16.Dn, 61.30.Eb

I. INTRODUCTION

A few years ago, Nastishin *et al.* [1] reported interesting results of a light-scattering study of pretransitional fluctuations in the isotropic phase of an aqueous solution of cromolyn (disodium cromoglycate), a lyotropic mesogen of disklike molecules which form elongated rods (aggregates) in aqueous solutions (see Refs. [2,3] and other relevant publications cited by Nastishin *et al.* [1]). The π-π interaction between the aromatic rings of the cromolyn molecules is considered a major driving force for the molecular face-to-face stacking. Upon cooling, such a solution separates into two phases, liquid crystalline and isotropic, undergoing a weakly first-order transition to the liquid crystalline phase. Depending on the cromolyn concentration, the liquid crystalline phase is either uniaxial nematic or columnar. Nastishin *et al.* [1] studied a cromolyn solution near the transition to the nematic phase. Above the transition temperature, T_{NI}, the homogeneous isotropic phase exhibits pronounced pretransitional fluctuations of the local anisotropy. By combining light-scattering and viscosity measurements, Nastishin *et al.* obtained the correlation length and average relaxation time of the local-anisotropy fluctuations and made an order-of-magnitude estimate of the cromolyn aggregate size. It was also speculated that the dramatic increase in the shear viscosity near the isotropic-nematic transition, observed in this system, is caused by elongation of the cromolyn aggregates upon cooling.

However, two important issues, which are of broader interest, remained unresolved. First, the mechanism of aggregation in lyotropic chromonic liquid crystals is still an open question. The possibility of characterizing the aggregation mechanism with dynamic light scattering as a function of temperature was not explored because the temperature range of the previous experiments was too narrow. Second, the previous study did not address a possible coupling between dynamic modes in this complex system. The signal/noise ratio of the measurements was not sufficient to make any definitive statements. Instead, Nastishin *et al.* [1] concluded that "further experimental studies of an expected coupling… are highly desirable."

The geometry of the cromolyn aggregates is very different from micelles, spherical or cylindrical, formed by amphiphilic (surfactant) molecules in regular lyotropic liquid crystals [2–4]. Structural x-ray data [5] suggest that cromolyn molecules in solution are arranged in cylindrical aggregates with the disks being predominately perpendicular to the axis of the cylinder. The intermolecular separation is about 0.34 nm along the aggregate axis, while the estimated cylinder diameter is about 2 nm. In contrast to closed micelles, the chromonic aggregates do not have a geometrically defined size, as there are no restrictions to adding another molecule to the existing stack. Therefore, at constant temperature the length of cromolyn aggregates is believed to increase continuously with increasing concentration. Such aggregation, also observed in studies of nucleic acid bases and nucleosides, is called "isodesmic" [2,3,6]. A Monte Carlo simulation of a model solution of chromonic and water "molecules" supports the mechanism of isodesmic aggregation [7]. Although there is no optimum length of the aggregation number with respect of the variation in chromonic concentration, at any given concentration the chromonic system is characterized by the average aggregation number that increases with increase in the concentration. A recent study of the absorption spectrum due to aggregation in a chromonic liquid crystal, the "Bordeaux dye," nicely describes the results with a simple model of isodesmic aggre-

*Corresponding author; anisimov@umd.edu

gation [6]. The tendency of the cromolyn molecules to aggregate was observed even in very dilute solutions [8], so that the chromonics were not believed to show a distinct threshold concentration, unlike the critical micelle concentration in amphiphilic systems [4]. However, in spite of the fundamental difference between the mechanisms of isodesmic aggregation and micellization, a recent NMR study of cromolyn in a phosphate buffer [9] indicated a sharp increase in the chemical shift at about 1 mass % of cromolyn, tempting the authors to controversially speak about the "critical self-association concentration" in the cromolyn solution. The chemical shift continued growing at higher concentrations, but much more gradually.

Moreover, effects of temperature on the mechanism of chromonic aggregation have not been investigated. Micellar (amphiphilic) systems, in addition to the critical micelle concentration threshold, commonly exhibit a temperature threshold for micellization, the "critical micellization temperature" [10,11]. After crossing the critical micellization temperature at constant concentration, the number of micelles grows at the expense of the monomers, while the average size of an individual micelle may not significantly change. A question arises whether the stacking of cromolyn molecules into aggregates may exhibit a temperature threshold (a "critical self-association temperature" analogous to the critical micellization temperature of amphiphilic molecules) and whether there are any effects of temperature on the size of the aggregates.

In this study we try to clarify the effects of temperature on the nature of self-assembly in the cromolyn solution with static and dynamic light scattering. In isotropic solutions, light is scattered due to the thermal fluctuations of density, concentration, and local anisotropy. The local anisotropy is associated with mutual orientations of anisotropic molecules or supramolecular aggregates. In the vicinity of the isotropic-nematic phase transition, the local anisotropy is characterized by the local nematic order parameter Q_{ij} (tensor of anisotropy [12–15]). The nematic order-parameter is a nonconserved variable. In the isotropic phase, where the average value of the order parameter $\langle Q_{ij} \rangle$ is zero, uncoupled fluctuations of the order parameter, δQ_{ij}, relax according to the simple relaxation dynamics [16],

$$\frac{\partial(\delta Q_{ij})}{\partial t} = -\frac{\delta Q_{ij}}{\tau}, \tag{1}$$

where t is time, and τ is the characteristic relaxation time (decay time) given by

$$\tau = \tilde{\eta}\chi, \tag{2}$$

where $\tilde{\eta}$ is a "rotational viscosity" and χ is the susceptibility with respect to the fluctuations of the nematic order parameter [14,17,18]. In principle, $\tilde{\eta}$, which controls the relaxation of anisotropy fluctuations, is different from the shear viscosity of the solution η, which controls the relaxation of velocity fluctuations. However, in many studies, these two friction coefficients are found to exhibit similar temperature dependences [14]. Although the equality is not guaranteed for all systems, our first approach, which can only be justified by comparison to experimental data, is to neglect any difference between them, whence $\tilde{\eta} \simeq \eta$. The three properties, τ_R, η, and χ, can be independently measured in the cromolyn solution with dynamic light scattering, a rheometer, and static light scattering, respectively [1]. Since Q_{ij} is a nonconserved variable, the inverse relaxation time τ^{-1} does not go to zero with the light-scattering wave number $q=(4\pi n/\lambda)\sin(\theta/2)$, where n is the refractive index, λ the wavelength of the incident light, and θ the scattering angle. However, τ does depend on q, through the susceptibility χ, which in general depends on q. The wave-number dependence of χ becomes significant when the correlation length ξ of the order-parameter fluctuations becomes comparable with q^{-1}. This happens close to a relevant second-order phase transition, where the susceptibility, as a function of the wave number, can be represented by the Ornstein-Zernike approximation [19],

$$\chi \simeq \frac{\chi_0}{1+\xi^2 q^2}, \tag{3}$$

where χ_0, the susceptibility in the "thermodynamic limit," can be obtained experimentally by extrapolating the corresponding intensity of light scattering, which is proportional to the susceptibility, to $q=0$. In the isotropic phase of a liquid crystal, ξ, in Eq. (3), is an effective correlation length resulting from two elastic terms in the Landau–de Gennes expansion of the free energy [20].

The concentration is a conserved variable. Uncoupled concentration fluctuations in a binary fluid, δc, relax in accordance with the diffusion dynamics [21],

$$\frac{\partial(\delta c)}{\partial t} = -\frac{\delta c}{\tau_D}, \tag{4}$$

with the explicitly q-dependent relaxation time,

$$\tau_D = \frac{1}{Dq^2}, \tag{5}$$

where D is the mutual diffusion coefficient. Therefore, the diffusion mode can be made arbitrarily slow by probing it at small enough values of q. In the previous study of Nastishin *et al.* [1], only a single diffusion mode was observed in the polarized light scattering. This mode was characterized with the diffusion dynamics of Eq. (4), and was interpreted as corresponding to the relaxation of concentration fluctuations of the cromolyn aggregates.

In this paper we present three results of a cromolyn study, with an improved light-scattering technique, to clarify the nature of the aggregation phenomena and the dynamic coupling of hydrodynamic modes. In the static light scattering we have observed the sudden onset of cromolyn aggregation below ~45 °C in 14% (mass) cromolyn solution. By more accurately separating the dynamic modes, which originate from the fluctuations of concentration and from the fluctuations of local anisotropy, we have observed three characteristic relaxation processes. We have observed two diffusion modes, "fast" and "slow," which are attributed to the diffusion of monomer-size particles and cromolyn aggregates, respectively. The diffusion coefficients of these two modes dif-

fer by an order of magnitude. Upon cooling, these two dynamic modes are observed to emerge from a single (fast) dynamic mode at about 44–46 °C corresponding to the onset of aggregation. The slow-diffusion mode does not significantly change between ~40° and the transition temperature of 32.7 °C, suggesting a stable average size of the cromolyn aggregates upon cooling. The third dynamic mode, associated with the relaxation of fluctuations in local anisotropy, is found to behave differently in the polarized and depolarized light scattering. In the polarized light-scattering alignment, the relaxation is described by uncoupled dynamics described by Eq. (1). In the depolarized light-scattering alignment, the experimental autocorrelation functions exhibit a strong q dependence, which is inconsistent with the simple relaxation dynamics of Eq. (1). This dependence can be quantitatively described by a theory [14,22] which accounts for a coupling between the fluctuations of local anisotropy and velocity fluctuations.

II. EXPERIMENTAL PROCEDURE

We have investigated the same sample of 14% (mass) cromolyn aqueous solution as was studied by Nastishin *et al.* [1]. The temperature of the transition to the nematic phase, T_{NI}, is found to be 32.7 °C, 0.9 °C higher than was reported four years ago. Although the optical cell was carefully sealed, the possibility of some subtle evaporation of water during the four-year period might explain the small transition-temperature shift. According to the phase diagram [23], a slight change in the cromolyn concentration from 14% to 14.2% would increase the transition temperature by about 1 °C. We have detected neither dust nor erosion of the glass surface of the cell.

The measurements have been performed with a custom-made PhotoCor spectrometer at 11 different scattering angles, from $\theta=15°$ to $\theta=150°$ with two settings of the analyzer: VV and VH; V and H denote vertical and horizontal polarizations of the incident and scattered light, respectively. We have significantly improved the resolution of the light-scattering instrument previously used to study pretransitional and critical fluctuations in aqueous and polymer solutions [1,24–27]. A new photon counting system with two photomultipliers, allows for cross correlations of two separate signals, which eliminates after-pulses and greatly increases the precision of the measurements of fast correlation times. For comparison and better confidence, the correlation functions were acquired with a PhotoCor-FC correlator and with an ALV-5000/E correlator. Analysis of the correlation functions was performed using both ALV-5000 and DYNALS (Alango/PhotoCor) software. We have also increased accumulation times (up to 1 h) and allowed for longer equilibration times between the temperature steps. The new measurements, taken over an extended temperature range, enabled us to detect the onset of cromolyn aggregation at about 45 °C.

Additionally, we made control measurements of static and dynamics light-scattering with a different experimental setup at a single temperature close to the phase transition. The optical cell in the alternative setup was submerged in an immersion liquid (decaline) that matches the refractive index of the optical glass with the surroundings to avoid stray light, thus making the angular measurements of light scattering more precise and reliable.

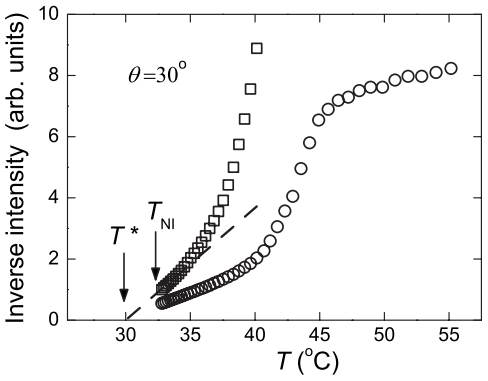

FIG. 1. Inverse intensity at the scattering angle $\theta=30°$ in the isotropic phase of the cromolyn solution as a function of temperature. The circles are experimental data for the vertically polarized light scattering (I_{VV}^{-1}) and the squares are for the depolarized light scattering (I_{VH}^{-1}). The dashed line shows the linear extrapolation which corresponds to the Landau–de Gennes behavior for the inverse nematic susceptibility χ_0^{-1},as given by Eq. (6), valid below 35 °C. The Ornstein-Zernike correction given by Eq. (3) is too small to be seen in the graph. The temperature $T^* \simeq 30$ °C is the absolute stability limit of the isotropic phase, $T_{NI} \simeq 32.7$ °C is the temperature of the isotropic-nematic transition.

III. STATICS DATA ANALYSIS

An example of our new measurements of the intensity of light scattering as a function of temperature in the isotropic phase of the cromolyn solution is shown in Fig. 1. The open circles indicate experimental data for the inverse intensity for the VV alignment (I_{VV}^{-1}) at $\theta=30°$. The total intensity I_{VV} includes both an anisotropic contribution $(I_{VV})_{an}$, due to fluctuations of the local anisotropy, and an isotropic contribution $(I_{VV})_{iso}$, due to concentration fluctuations of molecules and aggregates. The inverse intensity of the depolarized scattering (I_{VH}^{-1}), shown by squares, is only associated with fluctuations of the local anisotropy. The method of separating the anisotropic and isotropic light scattering in the VV alignment by using the experimental data for the depolarization ratio (I_{VH}/I_{VV}) is explained by Nastishin *et al.* [1].

It was also shown in Ref. [1] that, while $(I_{VV})_{iso}$ does not change much near the transition temperature T_{NI}, the intensity $(I_{VV})_{an}$ greatly increases and becomes proportional to the nematic (orientational) susceptibility. This susceptibility, the measure of the pretransitional nematic fluctuations, is described by Eq. (3). In the limit $q \to 0$ the susceptibility diverges at the temperature of the absolute stability limit of the isotropic phase T^* [14]. In accordance with the Landau–de Gennes theory [14], the nematic susceptibility in the isotropic phase, in the limit $q \to 0$, is

$$\chi_0 = \frac{l_0^3}{k_B(T - T^*)}. \tag{6}$$

In Eq. (6) k_B is Boltzmann's constant and l_0 is a characteristic length scale of the anisotropic molecules or anisotropic

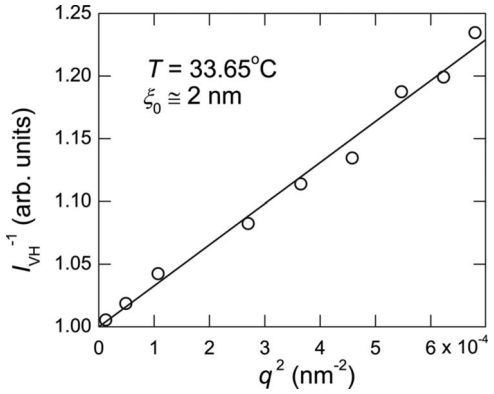

FIG. 2. An Ornstein-Zernike plot of the inverse intensity of the anisotropic scattering, obtained with the decaline immersion, in the isotropic phase of the cromolyn solution at 33.65 °C as a function the wave number.

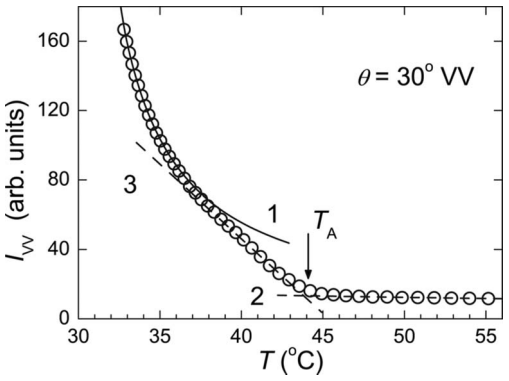

FIG. 3. The light-scattering intensity data for the vertically polarized light scattering (I_{VV}) at the scattering angle $\theta=30°$ in the isotropic phase of the cromolyn solution as a function of temperature. Three characteristic types of behavior are shown by the lines. Type 1 is the pretransitional scattering caused by near-critical fluctuations of local anisotropy (asymptotic Landau–de Gennes behavior); type 2 is the weakly temperature-dependent "molecular" scattering; and type 3 is the linear temperature dependence of the intensity, proportional to the number of the aggregates growing linearly with the temperature distance from $T_A \simeq 44$ °C.

supramolecular aggregates. Both I_{VV}^{-1} and $(I_{VV})_{an}^{-1}$ vanish, in the limit $q \to 0$, at the same temperature T^*. Therefore, the value of T^* can be obtained by an extrapolation to $q=0$, as demonstrated in Fig. 1. However, since $T_{NI}-T^* \simeq 10^{-2}T_{NI}$ is not a small temperature difference with respect to the range of the apparently linear behavior of (I_{VV}^{-1}), the linear extrapolation procedure is not very precise. Extrapolations of the intensity data obtained at different angles and for the different polarizations yield values of T^* varying from 29.4 °C (the value reported by Nastishin *et al.* [1]) to 30.5 °C. For this particular system we adopt the value of $T^*=30$ °C.

We have checked the wave-number dependence of the anisotropic light scattering for both VV and VH alignments of light scattering by using the alternative setup (with immersion) and confirmed that the pretransitional susceptibility indeed follows Eq. (3) as shown in Fig. 2. We have also confirmed the result, reported earlier by Nastishin *et al.* [1], that the correlation length of the pretransitional nematic fluctuations follows the Landau–de Gennes power law,

$$\xi \simeq \xi_0 \left(\frac{T-T^*}{T} \right)^{-1/2} \propto \chi_0^{1/2} \tag{7}$$

with $\xi_0 \simeq 2$ nm (close to the expected "diameter" of the rods) and $T^* \simeq 303$ K($\simeq 30$ °C). The measured correlation length is the same, within our experimental resolution, in the VH and VV alignments.

Both VV and VH intensity data clearly show a crossover from poor molecular light scattering above 45 °C to overwhelmingly "anisotropic" light scattering below 35 °C, with the intensity being proportional to the Landau–de Gennes susceptibility. In particular, this crossover unambiguously explains why the range of the validity of the Landau–de Gennes linear law in the cromolyn solution is so narrow.

As demonstrated in Fig. 3, the complex temperature dependence of the VV intensity can be separated into three parts. Above 45 °C the intensity is very low and is a weak function of temperature. We associate this part with the scattering by concentration fluctuations of monomer-size particles, such as cromolyn monomers or dimers and water molecules. The sharp increase in the intensity of light scattering below 45 °C signals the "onset" of cromolyn aggregation and indicates a relatively sharp transition from the molecular scattering to the scattering associated with the existence of anisotropic supramolecular aggregates. Between 42 and 36 °C the intensity increases nearly linearly with decreasing temperature, similar to the linear dependence observed by Bohorquez *et al.* [10] and Wu *et al.* [11] beyond a temperature-induced micellization threshold (at constant overall concentration) in nonionic amphiphilic copolymers. We can define a characteristic aggregation temperature $T_A \simeq 44$ °C at the intersection of lines 2 and 3 in Fig. 3. This is similar to the conventional definition of the critical micellization temperature [10,11]. The characteristic aggregation temperature corresponds to the inflection point of the inverse intensity shown in Fig. 1. Finally, below ~35 °C and down to the phase transition, the light scattering is mostly associated with near-critical fluctuations of local anisotropy and the temperature dependence of the intensity is well described by the Landau–de Gennes theory. The existence of the sudden onset of self-assembly in the cromolyn solution is also strongly supported by our new dynamic light-scattering measurements (as discussed in Sec. IV), which clearly show the emergence of a slow-diffusion mode (attributed to the diffusion of the cromolyn aggregates) upon cooling at about the same temperature of 45 °C.

The temperature dependence of the light-scattering intensity, shown in Figs. 1 and 3, cannot alone answer the question of whether the cromolyn aggregates continue to grow upon cooling or whether their average size remains stable. As compared with the viscosity of the solvent (water), the viscosity of the cromolyn aqueous solution demonstrates an anomalous growth (more than ten times) in a short temperature range of 8 °C [1]. Since such an anomaly does not usually exist in the isotropic phase of thermotropic nematics [17,18], Nastishin *et al.* [1] attributed this effect to the further elongation of supramolecular cromolyn aggregates when

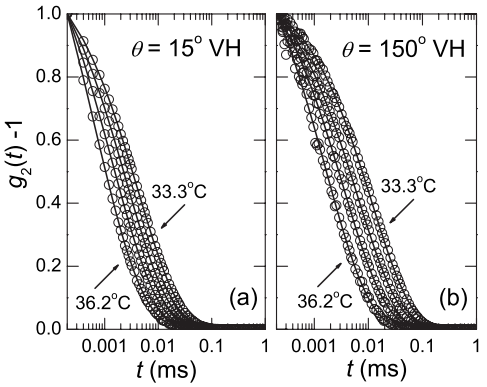

FIG. 4. Examples of the normalized dynamic intensity-autocorrelation functions $g_2(t)-1$ at $\theta=15°$ (a) and $\theta=150°$ (b) for depolarized light scattering at temperatures between 36.2 and 33.3 °C. Two sets of data between these two limits correspond to the temperatures 34 and 35 °C. The curves are obtained from fits of the correlation functions to stretched exponentials as given by Eq. (8).

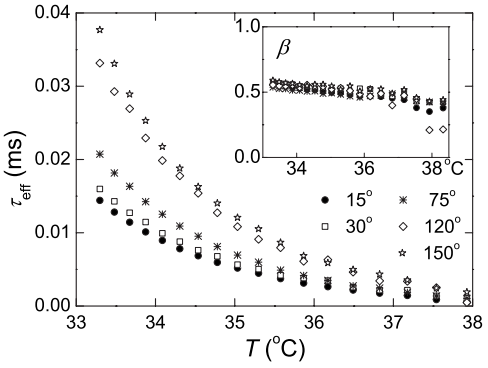

FIG. 5. The temperature dependences of the effective decay times of the anisotropy fluctuations in the cromolyn solution obtained for the depolarized light scattering at different scattering angles from fits to Eq. (8). The inset shows the temperature dependence of the stretching parameter β.

the temperature decreases. However, the new dynamic data show that the average length of the aggregates saturates at about 40 °C and remains stable upon further cooling.

IV. DYNAMICS DATA ANALYSIS

A. Depolarized light scattering

In complex solutions of anisotropic scatterers, the analysis of the relaxation dynamics is complicated by the presence of multiple dynamic modes, especially in the VV alignment, where both isotropic and anisotropic scattering contribute to the dynamic intensity-autocorrelation functions [29–33]. For this reason, we first consider the data from the VH alignment, where isotropic scattering is not present. The VH results are subsequently used to clarify and interpret the VV results.

Eight examples of the experimental intensity-autocorrelation functions obtained in the VH alignment are shown in Fig. 4. The decay times of the correlation functions clearly exhibit the expected critical slowing down upon cooling. However, the dependence of the relaxation time on the scattering angle is inconsistent with the uncoupled dynamics described by Eq. (1). Although some angular dependence of the decay times is expected to originate from the Ornstein-Zernike susceptibility given by Eq. (3), this should lead to a decrease in the relaxation time with increasing scattering angle, not the increase seen in Fig. 4.

The analysis of the experimental correlation functions presented in Fig. 4 has shown that the functions do not decay as single exponentials. However, the correlation functions for all of the angles studied are well fit to stretched exponentials as

$$g_2(t) - 1 = \exp\left[-2\left(\frac{t}{\tau_{\text{eff}}}\right)^{\beta}\right]. \tag{8}$$

The fits are shown in Fig. 4 by the solid curves. Figure 5 presents the effective relaxation times τ_{eff}, as functions of temperature, obtained from the single stretched exponential fits at five angles. The effective relaxation times are seen to increase monotonically with increasing scattering angle at all temperatures, in contradiction to the expected Ornstein-Zernike behavior. The effective stretching parameter β, shown as an inset in Fig. 5, demonstrates only a weak temperature dependence, varying from 0.4 (far from the transition) to 0.6 (close to the transition) and is almost independent of the scattering angle. These values are similar to those reported for high-molecular-weight polymer solutions [24,34] and for other solutions of disklike lyomesogens [28].

To explain the seemingly unusual q dependence of the dynamic correlation function in the VH alignment we consider a possible coupling between hydrodynamics modes, an effect not included in the simple relaxation dynamics of Eq. (1). We note that, in general, the normalized dynamic intensity-autocorrelation function of the fluctuations of anisotropy for depolarized light scattering is given by [29],

$$g_2(t) - 1 \propto \left[\langle \delta Q^*_{xy} \delta Q_{xy}(t)\rangle \sin^2\left(\frac{\theta}{2}\right) + \langle \delta Q^*_{yz} \delta Q_{yz}(t)\rangle \cos^2\left(\frac{\theta}{2}\right)\right]^2, \tag{9}$$

where t is time. This expression results from a choice of scattering geometry in which the incident beam propagates in the xz plane, polarized in the y direction, with wave vector $\mathbf{k}_i$, the scattered beam propagates in the xz plane, polarized in the xz plane, with wave vector $\mathbf{k}_f$, and the scattering geometry is selected such that the scattering vector $\mathbf{q} \equiv \mathbf{k}_i - \mathbf{k}_f$ points in the negative z direction, i.e., $\mathbf{q} = -q\hat{\mathbf{z}}$. For the uncoupled relaxation dynamics described by Eq. (1), the two correlation functions, $\langle \delta Q^*_{xy} \delta Q_{xy}(t)\rangle$ and $\langle \delta Q^*_{yz} \delta Q_{yz}(t)\rangle$ are identical. In this case, the $\sin^2(\frac{\theta}{2})$ and $\cos^2(\frac{\theta}{2})$ add to unity and do not contribute to the q dependence of $g_2(t)-1$. However, if the two correlation functions in Eq. (9) decay with different characteristic relaxation times, $\sin^2(\frac{\theta}{2})$ and $\cos^2(\frac{\theta}{2})$ will contribute to the q dependence of $g_2(t)-1$. In fact, Eq. (9) implies that the effective relaxation time of $g_2(t)-1$ will increase with scattering angle, the effect seen in Fig. 5, if $\langle \delta Q^*_{xy} \delta Q_{xy}(t)\rangle$ decays more slowly than $\langle \delta Q^*_{yz} \delta Q_{yz}(t)\rangle$.

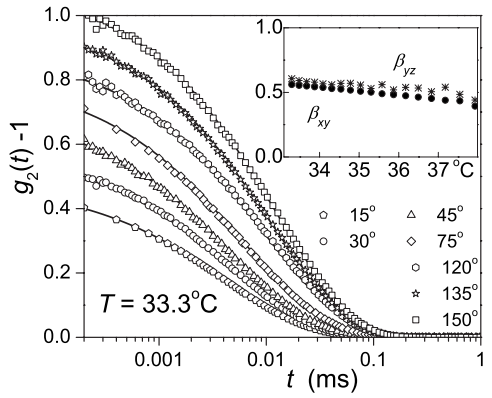

FIG. 6. Examples of the normalized dynamic intensity-autocorrelation functions $g_2(t)-1$ for depolarized light scattering at 33.3 °C obtained at different scattering angles. The theoretical curves for 15° and 150° are obtained from fits to Eq. (10). The curves for the intermediate angles are predictions given by Eq. (10) without adjustable parameters. The inset shows the temperature dependence of the stretching parameters β_{yz} and β_{xy} obtained from the fits to Eq. (10) at 15° and 150°.

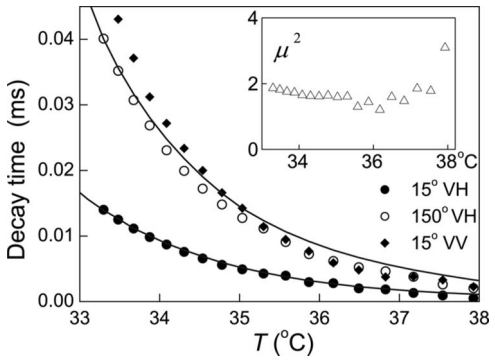

FIG. 7. The temperature dependence of the decay time of the anisotropy fluctuations $\tau/(1+\mu^2)$ coupled with velocity fluctuations for the depolarized light scattering at $\theta=15°$ (solid circles), the decay time τ obtained for the depolarized scattering at $\theta=150°$ (open circles), and the decay time τ obtained for the polarized light scattering at $\theta=15°$ (solid diamonds). The upper curve is τ obtained from a fit to Eq. (13) and the lower curve is $\tau/(1+\mu^2)$ obtained assuming a constant μ. The coupling parameter μ^2 as a function of temperature is shown in the inset.

The preceding discussion suggests that the experimental correlation functions can be fit by Eq. (9) with the correlation functions represented by stretched exponentials, yielding

$$g_2(t)-1=\left\{\exp\left[-\left(\frac{t}{\tau_{xy}}\right)^{\beta_{xy}}\right]\sin^2\left(\frac{\theta}{2}\right)+\exp\left[-\left(\frac{t}{\tau_{yz}}\right)^{\beta_{yz}}\right]\cos^2\left(\frac{\theta}{2}\right)\right\}^2. \tag{10}$$

We have fit all the experimental correlation functions from the depolarized scattering to Eq. (10). An example of the fitting procedure is presented in Fig. 6. The solid curves in Fig. 6 were first obtained by fitting the correlation functions for 15° and 150° in order to extract τ_{xy}, τ_{yz}, and the stretching parameters β_{xy} and β_{yz}. All of the solid curves, corresponding to intermediate angles, were then predicted with use of the parameters extracted for 15° and 150° and the Ornstein-Zernike correction $\tau/\tau_{q=0}=(1+\xi^2q^2)^{-1}$. In Fig. 6 the correlation functions and corresponding fits are given arbitrary normalizations to clearly separate the data from different scattering angles. The same level of agreement with Eq. (10) is seen for all temperatures. This indicates that Eq. (10) accounts for all of the q dependence of the experimental correlation functions. The stretching parameters β_{xy} and β_{yz}, shown as an inset in Fig. 6, are very close to each other and very similar to the effective stretching exponent β shown in Fig. 5.

The unconventional q dependence of τ_{eff} seen in Fig. 5 is completely accounted for by Eq. (10), without having to abandon the Ornstein-Zernike susceptibility. The effect of the Ornstein-Zernike susceptibility, which tends to decrease τ (or τ_{xy} and τ_{yz}) with increasing q, is much weaker than the q dependence due to the mixing of correlation functions in Eq. (10), which tends to increase the effective relaxation time τ_{eff} with q. For our system and choice of experimental scattering angles, the Ornstein-Zernike correction to the susceptibility will change the relaxation time by at most 20% for the lowest temperature, where τ_{xy} is over twice larger than τ_{yz} [see Fig. 7]. The fact that τ_{xy} and τ_{yz} differ by a factor of 2 and are not separated by an order of magnitude explains why the single stretched exponential fit provides a good approximation to the correlation function Eq. (10). While the effects of the q dependences from the mixing and the susceptibility tend to counteract each other, the effect from the mixing overpowers the effect from the Ornstein-Zernike correction in the susceptibility, resulting in the overall increase in τ_{eff} with q.

Equation (10) is consistent with a theory which incorporates a linear coupling between local-anisotropy fluctuations and velocity fluctuations. Systems composed of anisotropic components are known to exhibit a birefringence under steady shear. The same physics in the isotropic phase of liquid crystals is manifested through a coupling between velocity fluctuations and molecular orientations [14]. This coupling affects the relaxation of the local-anisotropy fluctuations in such a way that the dynamic correlations of the local anisotropy are given by

$$\langle \delta Q_{xy}^*\delta Q_{xy}(t)\rangle = C\exp\left(-\frac{t}{\tau}\right), \tag{11}$$

$$\langle \delta Q_{yz}^*\delta Q_{yz}(t)\rangle = C\exp\left(-\frac{1+\mu^2}{\tau}t\right), \tag{12}$$

where μ is a dimensionless Onsager coefficient that couples the local-anisotropy production rate to the velocity fluctuations, and where the amplitude is given by $C=k_BT\chi/l_0^3$. Equations (11) and (12) imply that $\langle \delta Q_{yz}^*\delta Q_{yz}(t)\rangle$ always relaxes with a smaller relaxation time than $\langle \delta Q_{xy}^*\delta Q_{xy}(t)\rangle$. A brief review of the derivation of Eqs. (11) and (12) is presented in the Appendix.

In arriving at Eqs. (11) and (12), we have assumed that the velocity fluctuations relax much faster than the local-anisotropy fluctuations. Typical anisotropy relaxation times in the system are on the order of $10^{-1}-10^{-2}$ ms (see Fig. 5). The relaxation time for the velocity fluctuations is characterized by the q-dependent shear relaxation time, $1/\nu q^2 \simeq 10^{-4}-10^{-8}$ ms (where ν is the kinematic viscosity). The upper bound of this range corresponds to the viscosity of the solvent and the scattering angle $\theta=15°$. Even at the extreme values of the relaxation times for our experimental conditions, the inequality $1/\nu q^2 \ll \tau$ holds.

It is not clear whether the stretched exponential decay in the system is due to nonlinear interactions between hydrodynamic modes or polydispersity in aggregate lengths, and therefore relaxation times. In other systems, polymers solutions near-critical demixing [24,34] for example, where stretched exponential decays are experimentally observed, the authors have found good agreement between theory and experiment simply by adding the stretching parameter to the theoretical single exponentials. Therefore, we will assume that, in Eq. (10), the obtained relaxation times $\tau_{xy} \simeq \tau$ and the $\tau_{yz} \simeq \tau/(1+\mu^2)$. The validity of these assumption is justified by comparison with the experimental data.

The temperature dependences of τ, $\tau/(1+\mu^2)$, and μ^2 are presented in Fig. 7. The open circles correspond to τ and the solid circles correspond to $\tau/(1+\mu^2)$. The solid diamonds represent the orientational relaxation time obtained in the polarized scattering; they will be addressed in Sec. V. The values for μ^2 were found by taking the ratio of the experimentally measured decay times τ and $\tau/(1+\mu^2)$. The temperature dependence of the "uncoupled" relaxation time τ is in good agreement with the well-known prediction for the pretransitional relaxation of anisotropy fluctuations in liquid crystals [14,17,18] given by Eq. (2). To account for the deviation of the temperature dependence of the susceptibility from the asymptotic Landau–de Gennes behavior given by Eqs. (6) and (3), we express Eq. (2) as

$$\tau = \eta\chi \simeq \frac{\eta l_0^3}{k_B(T_{\mathrm{NI}} - T^*)} \frac{I(T)}{I(T_{\mathrm{NI}})}, \tag{13}$$

where χ is the pretransitional nematic susceptibility, $T^* \simeq 303$ K (as obtained from the static light scattering), $I(T)$ is the experimental VH intensity, T_{NI} is the transition temperature at which the experimental VH intensities are normalized to 1, and $l_0 \simeq 6.4$ nm is the characteristic length of the anisotropic aggregates as defined by Eq. (6). The viscosity data are taken from Ref. [1], where the shear viscosity is approximated by the Vogel-Fulcher equation,

$$\eta = \eta_0 \exp\left(\frac{B}{T - T_0}\right), \tag{14}$$

with the fitting parameters $\eta_0=0.0136$ mPa s, $B=130$ K, and $T_0=286$ K (the temperature of the apparent divergence of the viscosity).

B. Polarized light scattering

With our assessment of the dynamics of the orientational fluctuations obtained in the VH alignment, the rather complicated dynamics picture seen for the VV alignment is easier to interpret. Using the standard regularization procedure for inverse Laplace transforms (see Ref. [24] for details), we have calculated the decay-time distributions $H(\tau)$ from the VV correlation functions. The decay-time distributions model the relaxation process as a superposition of exponentials such that $g_2(t)-1=[\int H(\tau)e^{-t/\tau}d\tau]^2$. The distributions obtained for a sequence of temperatures are combined in a single plot, in which the distribution maxima at different temperatures join to form "ridges." The distribution plots are useful because they are able to locate the dominant dynamic modes in the system without reference to a specific relaxation model. An example of a decay-time distribution, obtained in the VV alignment for the scattering angle 30°, is shown as a contour map in Fig. 8. The contour lines join decay times of equal distribution magnitude at different temperatures.

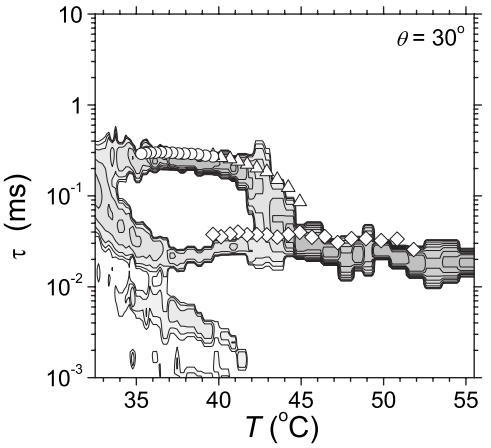

FIG. 8. Decay time distributions for the VV alignment of light scattering in the isotropic phase of the cromolyn solution at $\theta=30°$ over the broad temperature interval. The contour lines join decay times of equal distribution magnitude. The symbols represent the results obtained by the fits to Eqs. (15) and (16) above 45 °C and between 40 and 45 °C, respectively. Diamonds are used for the fast-diffusion time and triangles are used for the slow-diffusion time. Below 40°, the slow-diffusion time (circles) is obtained from fits to a single exponential in the time domain above 0.1 ms. The emergence of the slow-diffusion mode at about 45 °C is attributed to the onset of cromolyn aggregation.

At all eleven scattering angles studied, we have observed a single pronounced ridge in the decay-time distributions above 45 °C. The relaxation time associated with this ridge is only weakly temperature dependent. We interpret this ridge as corresponding to the (fast) diffusion of cromolyn-monomer size particles in water. For temperatures below 45 °C, a second pronounced ridge is observed to emerge from the fast-diffusion ridge. The relaxation time associated with this mode decreases rapidly over a temperature interval of several degrees and then saturates. We interpret this ridge as corresponding to the diffusion of cromolyn aggregates. A third dynamic mode appears just below 45 °C. This mode is broader than either of the two diffusion modes, especially at higher temperatures. The relaxation times associated with this mode are initially much smaller than the diffusion times. As the transition temperature is approached, the relaxation

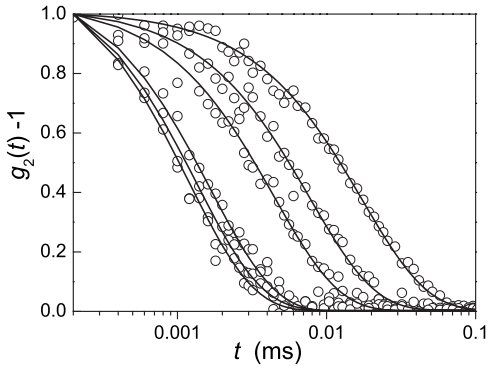

FIG. 9. Dynamic intensity-autocorrelation functions for the VV alignment at 49 °C for different scattering angles. The curves are obtained from the fits to single exponentials.

time of this third mode slows down significantly, eventually becoming comparable to both of the diffusion times. We interpret this third mode as corresponding to the relaxation of fluctuations of the local anisotropy.

The preceding interpretation is supported by a direct analysis of the dynamic autocorrelation functions. Examples of the correlation functions at 49 °C are shown in Fig. 9. At temperatures above 46 °C, the correlation functions are well described by a single exponential,

$$g_2(t) - 1 = \left[A_1 \exp\left(- \frac{t}{\tau_{D_1}} \right) \right]^2, \tag{15}$$

where A_1 is the amplitude. If a stretched exponential is used, the stretching parameters are found to be close to one. Below the onset of aggregation the slow-diffusion mode emerges. Examples of the VV correlation functions at 30°, for several temperatures between 46 and 36 °C, are shown in Fig. 10. In the interval from 46 to 45 °C there is qualitative evidence for the existence of two diffusion modes, but the diffusion times are too close to allow for a stable fit to two exponentials. However, between 45 and 40 °C, a good fit to two exponentials as

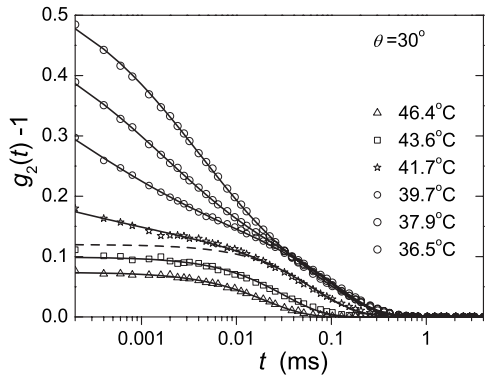

FIG. 10. Examples of dynamic intensity-autocorrelation functions for the VV alignment at θ=30°. The initial amplitude of the correlation functions is given by the static intensity correlation function. The curves are obtained from the fits to Eqs. (15) at 46.4 °C, (16) at 41.7 °C, and (17) at 39.7, 37.9, and 36.5 °C. The dashed curve is the fit to the single exponential slow diffusion.

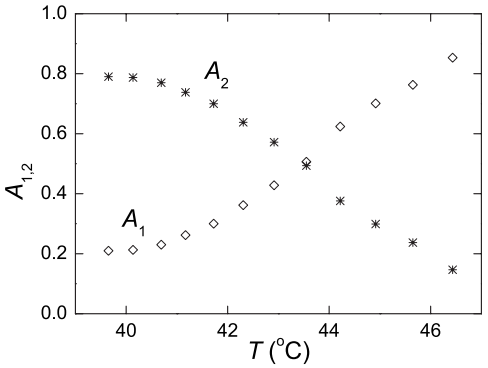

FIG. 11. The normalized amplitudes from the fits to Eq. (16) at θ=30° VV. The amplitude A_1 corresponds to the fast-diffusion mode, and the amplitude A_2 corresponds to the slow-diffusion mode. At the end of the aggregation process the slow diffusion has become the dominate mode at the expense of the fast-diffusion mode.

$$g_2(t) - 1 = \left\{ A_1 \exp\left[- \left(\frac{t}{\tau_{D_1}} \right) \right] + A_2 \exp\left[- \left(\frac{t}{\tau_{D_2}} \right) \right] \right\}^2 \tag{16}$$

is obtained. In Eq. (16) A_1 and A_2 are amplitudes for the fast- and slow-diffusion modes, respectively. The two-exponential decay signals the emergence of the slow-diffusion mode. Below 45 °C, a contribution to the correlation functions from the orientational mode is also present. However, between 45 and 40 °C, the orientational mode is faster and much weaker than the diffusion modes, so that our fit to only two exponentials is a reasonable approximation. The diffusion times, obtained from the two-exponential fits and plotted along with the distribution of decay times in Fig. 8, are in agreement with the positions of the maxima. The temperature dependences of the amplitudes A_1 and A_2 are presented in Fig. 11, where the crossover from monomer-size molecular scattering above 45 °C to mainly aggregate scattering below 45 °C is evident.

Below $T \simeq 40$ °C, it is no longer possible to resolve the contribution of the fast-diffusion mode, while the influence of the growing orientation mode begins to be significant. At T=41.7 °C, this effect is first seen in Fig. 10 as a slight kink in the correlation function away from single exponential decay, shown by the dashed curve, for small times. Upon further cooling the relative amplitude of the orientation mode continues to increase and the orientational relaxation time continues to grow. For the temperatures below 40 °C we have fit the experimental correlation functions to the sum of a single exponential and a stretched exponential,

$$g_2(t) - 1 = \left\{ A_1 \exp\left[- \left(\frac{t}{\tau_{D_1}} \right) \right] + A_3 \exp\left[- \left(\frac{t}{\tau} \right)^{\beta} \right] \right\}^2, \tag{17}$$

where A_3 is the amplitude of the orientational mode. It is seen from Fig. 10 that for times greater than $t \simeq 0.03$ ms the

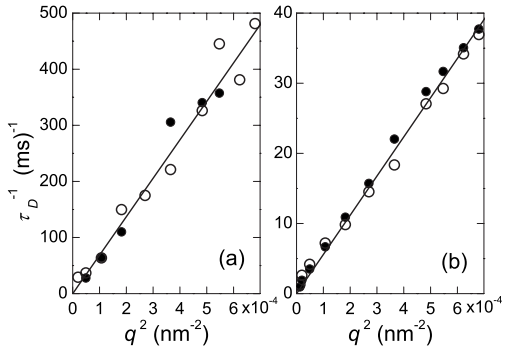

FIG. 12. Wave-number dependence of the diffusion rates for fast diffusion (a) and slow diffusion (b). Open circles are obtained from the maxima of the decay-time distributions. Solid circles are the results of the fits to single exponentials. Solid lines indicate the approximation given by Eq. (5).

correlation functions collapse onto each other, indicating that the main contribution to the correlation functions in this time domain is the saturated slow-diffusion mode. For times less than $t \simeq 0.03$ ms, the orientational mode is the dominant contribution to the correlation functions.

1. Diffusion modes in the polarized light scattering

The decay rates of the aggregate and monomer diffusion differ from each other by one order of magnitude. Both of the diffusion relaxation times are found to be consistent with Eq. (5). The diffusion coefficients for the fast (monomer size) mode (D_1) and slow (aggregates) mode (D_2) are obtained from the slopes of $1/\tau_{D_{1,2}}$ versus q^2 plots as shown in Fig. 12. The points on these plots are taken from both the distribution analysis and the multiexponential fits. For the fast-diffusion time [Fig. 12(a)], the filled circles represent the average diffusion times taken from the single exponential fits above 45 °C. In Fig. 12(b), the closed circles represent slow-diffusion times taken from fits of the correlation functions to the two-exponential decay given by Eq. (16). The open circles in Figs. 12(a) and 12(b) are taken from the decay-time distributions below 45 °C.

The diffusion coefficient for each diffusion mode was approximated with the Stokes-Einstein expression as [21]

$$D_{1,2} \simeq \frac{k_B T}{6\pi\eta_s R_{1,2}}, \tag{18}$$

where η_s is the solvent (water) viscosity, and $R_1 \simeq 0.5$ nm and $R_2 \simeq 6.3$ nm are the effective hydrodynamic radii. It is remarkable that the value of R_2 is so close to the length $l_0 \simeq 6.4$ nm obtained from our fit of the orientational relaxation τ to Eq. (13), while R_1 is on the order of the cromolyn-monomer radius. The lengths $R_{1,2}$ give only order-of-magnitude estimates of the characteristic size of the cromolyn aggregates since the diffusion of nonspherical aggregates cannot be quantitatively described by the Stokes-Einstein expression. A more sophisticated expression for the diffusion coefficient (e.g., see the discussion in [35]) is not necessary to distinguish changes in the size of the aggregates.

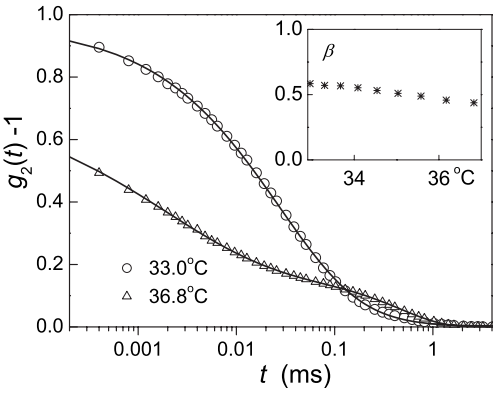

FIG. 13. Two examples of dynamic intensity-autocorrelation functions for the VV alignment at $\theta = 15°$. The solid curves in the figure were obtained from fits to Eq. (17). The inset shows the stretching parameters obtained from these fits.

It is clear from Eq. (18) that the sharp slowing down of the aggregate diffusion mode seen in Fig. 8, corresponds to the elongation of rodlike aggregates within a narrow temperature interval of a few degrees below 45 °C. This elongation virtually saturates below this interval. Both diffusion modes depend weakly on temperature, after the slow-diffusion mode has saturated, suggesting that the length of the aggregates does not significantly change upon cooling and that the diffusion of the monomers and aggregates is mainly affected by the solvent viscosity. Therefore, the anomalous growth of the solution viscosity reported in [1], cannot be explained by the elongation of the cromolyn aggregates.

2. Orientational relaxation mode in the polarized light scattering

The wave-number dependence of the orientational mode in the VV alignment is more difficult to resolve than that of the diffusion modes. For most experimental angles the orientational relaxation time is comparable to the slow-diffusion time near the transition. This problem is particularly exacerbated at large scattering angles, when the q-dependent diffusion modes overlap the orientational mode for a broad range of temperatures. Only at $\theta = 15°$ are the time scales for the orientational mode and the slow-diffusion mode different enough to separate them unambiguously at all temperatures below 37 °C. Two examples of experimental correlation functions at 15° are shown in Fig. 13. For $T = 36.8$ °C the contribution to the experimental correlation function from two distinct decay processes is clearly evident. At $T = 33$ °C, the contribution from the diffusion mode has been overwhelmed by the orientational mode. We have fit the experimental correlation functions at 15° to a combination of a single exponential and a stretched exponential given by Eq. (17) where A_2 and A_3 are normalized amplitudes. The stretching parameters, which are found to be very similar to those seen in the VH alignment, are plotted as an inset in Fig. 13. The amplitudes A_2 and A_3 are plotted in Fig. 14. Clearly, the orientation mode becomes much stronger than the diffusion mode at lower temperatures.

V. DISCUSSION

As recently discussed by Tomasik and Collings [6], there are two alternative mechanisms of aggregation phenomena in

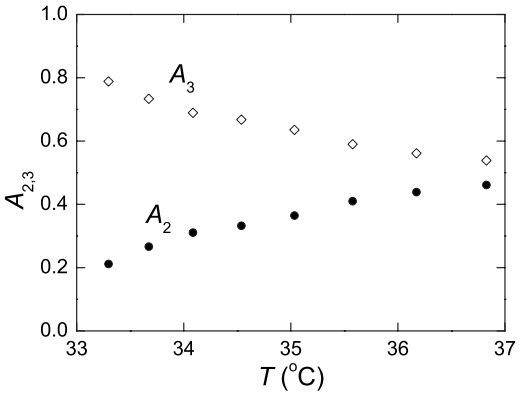

FIG. 14. The normalized amplitudes from the fits to Eq. (17) at $\theta=15°$ VV. The amplitude A_2 corresponds to the slow-diffusion mode, and the amplitude A_3 corresponds to the orientational mode.

lyotropic liquid crystals. One is micellization, through which amphiphilic molecules form micelles above the "critical micellization concentration" or below the "critical micellization temperature." A further increase in amphiphilic concentration or a decrease in the temperature results in an increase in the number of micelles, while their size may remain relatively stable. Cromolyn solutions are assumed to belong to another type of lyotropic liquid crystal in which the solute molecules are disklike and only weakly amphiphilic. In water, the cromolyn molecules may tend to aggregate into stacks through "isodesmic aggregation." As the concentration increases, the distribution of aggregates shifts to higher aggregation numbers and the aggregates are elongated [6,7] at the expense of the cromolyn monomers. One might assume a similar process occurred in our system upon cooling with no distinct "aggregation temperature." However, our experiments, both static and dynamic, show that there is a relatively sharp aggregation threshold at about 45 °C (for 14% solution) indicating that in the cromolyn solution the isodesmic aggregation phenomena may occur in a very narrow temperature interval of about 3–4 °C. Moreover, we do not find any evidence of significant elongation of the aggregates outside of this temperature interval. A microscopic model that describes such a sharp isodesmic aggregation in a narrow temperature interval is yet to be developed.

The pretransitional slowing down in the cromolyn solution, observed in the depolarized light scattering (VH), strongly depends on the light-scattering wave number q. The relaxation time increases with an increase of q. We interpret this effect as resulting from coupling between the fluctuations of local-anisotropy and velocity fluctuations. While, in general, for systems of anisotropic scatterers, such a coupling is expected, the strength and consequences vary. This coupling was intensively studied for systems of anisotropic molecules, like anisaldehyde, in the "fast reorientation" limit $1/\nu q^2 \gg \tau$ [29]. The theory of the velocity-anisotropy coupling has also been developed in the "slow reorientation" limit, $1/\nu q^2 \ll \tau$ [14]. As previously mentioned, the slow reorientation limit applies to the cromolyn solution because the orientational relaxation becomes increasingly slow as the isotropic-nematic transition is approached.

We have thus far used the Onsager cross-coupling coefficient μ to characterize the velocity-anisotropy coupling. However, the velocity-anisotropy coupling is often, in the literature, characterized by a parameter R [29], which is related to μ by $R=\mu^2/(1+\mu^2)$. While μ can vary from 0 to ∞, R varies between 0 and 1. Two theories for R have been developed using molecular hydrodynamics for slip boundary conditions and stick boundary conditions. For the stick boundary conditions R depends on the geometric (shape) anisotropy of the molecules as $R \propto \epsilon^2/(2+\epsilon)^2$, where ϵ is the shape anisotropy of the particles [36]. In contrast, for slip boundary conditions, R is independent of shape anisotropy [37]. Using our experimental values for μ we find that our R values range is $R \simeq 0.45-0.65$. These values are generally larger than those found in systems with small anisotropy, but smaller than those reported for a semiflexible polymer [38,39], $R \simeq 0.8$.

The orientational relaxation time found for $\theta=15°$ in the polarized light-scattering alignment is plotted together with the relaxation times obtained with the depolarized scattering in Fig. 7. The relaxation times for $\theta=15°$ in the polarized scattering are much closer to the relaxation times (almost uncoupled) seen at $\theta=150°$ in the depolarized scattering than to the relaxation times (coupled) at $\theta=15°$ in the depolarized scattering. This finding is consistent with our interpretation of the correlation functions in the depolarized scattering alignment and the corresponding theory of coupling between the fluctuations of local anisotropy and velocity. In the VV geometry, light scattering only probes fluctuations in the Q_{yy} component of the local anisotropy [29]. Unlike the components probed in the VH geometry, δQ_{yy} does not couple to velocity fluctuations. Therefore, the orientational mode seen in the VV geometry should correspond to the uncoupled mode with the characteristic relaxation time given by Eq. (13). At lower temperatures, the relaxation time τ obtained at $\theta=15°$ for polarized scattering is slightly larger than τ obtained at $\theta=150°$ for depolarized light scattering. This effect is qualitatively consistent with the Ornstein-Zernike correction to the susceptibility, however, an additional q dependence of the susceptibility associated with the existence of two correlation lengths ξ_1 and ξ_2 [20], as discussed in the Appendix, could also contribute to this difference.

As compared with the viscosity of the solvent (water), the viscosity of the cromolyn solution demonstrates an anomalous growth upon approaching the transition temperature T_{NI}. Such an anomaly does not usually exist in the isotropic phase of thermotropic nematics [17]. The Vogel-Fulcher equation [see Eq. (14)] is a generalization of the standard Arrhenius equation (in which $T_0=0$) and is commonly applied to liquids exhibiting a glass transition [40]. Interestingly, a glass-like character of molecular ordering was also found in another solutions of disklike lyomesogens [28]. However, a coupling between the orientational fluctuations and velocity fluctuations, and consequently a q-dependent VH dynamic mode, was not observed in Ref. [28], probably because the pretransitional slowing down was not present in the system. The fact, that the average length of the cromolyn aggregates below 40 °C does not significantly change, reaching 6–7 nm, and the fact that the temperature dependence of translational diffusion coefficient is controlled by the solvent (water) viscosity, suggests that the anomalous growth of the shear viscosity in the cromolyn solution is not caused by the

elongation of cromolyn aggregates and could be related to the emergence of glasslike behavior upon cooling.

VI. CONCLUSIONS

Using an improved light-scattering technique we have observed several new features of the pretransitional fluctuations in the isotropic phase of a lyotropic liquid crystal, the cromolyn solution previously studied by Nastishin *et al.* [1]. We have detected the onset of cromolyn aggregation induced by decreasing temperature by both static and dynamic light scattering. This new result favors an interpretation in which the isodesmic aggregation (continuous stacking) of cromolyn molecules into aggregates with a characteristic length of 6–7 nm only develops over a narrow temperature interval of a few degrees and saturates below this interval. By separating contributions from the fluctuations of concentration and local anisotropy, multiscale dynamics of the fluctuations have been observed in the polarized and depolarized light scattering. The results from the polarized light scattering (VV) indicate that in addition to the previously reported slow-diffusion mode, interpreted as the diffusion of the cromolyn aggregates, there is a fast-diffusion mode corresponding to the diffusion of the cromolyn monomers. Both diffusion modes are controlled by the viscosity of the solvent (water) which is much smaller than the actual viscosity of the solution near the transition temperature. In the depolarized light scattering (VH) we have observed a strong, q-dependent mode associated with the relaxation of the local-anisotropy fluctuations. The q dependence of this mode is quantitatively described by a coupling between fluctuations of the local-anisotropy and velocity fluctuations. In the polarized light scattering (VV) the relaxation of the local-anisotropy fluctuations is uncoupled since in this geometry the light scattering only probes fluctuations in the uncoupled component of the local-anisotropy tensor, which is in agreement with the existing theory [29].

ACKNOWLEDGMENTS

This study was made possible due to our past collaboration with Yu. A. Nastishin, H. Liu, S. V. Shiyanovskii, and O. D. Lavrentovich [1]. We thank P. Collings for sending us the preprint of Ref. [6] and for fruitful discussions, and I. K. Yudin and V. A. Dechabo for helping us with improving the light-scattering technique. We also appreciate useful comments made by J. V. Sengers.

APPENDIX: THE CORRELATION FUNCTION OF COUPLED LOCAL-ANISOTROPY FLUCTUATIONS

de Gennes and Prost have presented a hydrodynamic theory that describes the effect of local velocity-anisotropy coupling on the dynamics of pretransitional fluctuations in the isotropic phase of liquid crystals [14,43]. A similar but more rigorous derivation can be made with "fluctuating hydrodynamics" [41,42]. The main results of this derivation, Eqs. (A7) and (A8), are identical to those found by other authors using different methods [29].

In the context of fluctuating hydrodynamics, the derivation of the dynamic autocorrelation functions $\langle \delta Q_{xy}^{*} \delta Q_{xy}(t) \rangle$ and $\langle \delta Q_{yz}^{*} \delta Q_{yz}(t) \rangle$ begins with balance laws expressing the nonconservation of the local anisotropy and the conservation of the local momentum density,

$$\frac{\partial(\delta Q_{ij})}{\partial t} = \Phi_{ij},$$

$$\rho \frac{\partial(\delta v_i)}{\partial t} = -\nabla_j \Pi_{ij}, \tag{A1}$$

where δQ_{ij} and δv_{ij} are equilibrium fluctuations of the local anisotropy and velocity, Φ_{ij} and Π_{ij} are the local-anisotropy production rate and the momentum density flux, and ρ is the mass density of the solution. The preceding equations are linearized in both δQ_{ij} and δv_i since we are only interested in fluctuations around the equilibrium state defined by $Q_{ij}=0$ and $v_i=0$.

In order to close the above system of equations, it is necessary to introduce a set of linearized phenomenological relationships between the fluctuating forces and the fluxes given by

$$\Phi_{ij} = -\frac{1}{\tilde{\eta}\chi_0}\delta\tilde{Q}_{ij} + \frac{\sqrt{2}\mu}{2}(\nabla_i \delta v_j + \nabla_j \delta v_i) + \delta\Phi_{ij},$$

$$\Pi_{ij} = -\frac{\sqrt{2}\mu}{\chi_0}\delta\tilde{Q}_{ij} - \eta(\nabla_i \delta v_j + \nabla_j \delta v_i) + \delta\Pi_{ij}, \tag{A2}$$

where $\delta\Phi_{ij}$ and $\delta\Pi_{ij}$ are the fluctuating part of the local-anisotropy production rate and the fluctuating part of the momentum density flux, η is the solution viscosity, χ_0 is the susceptibility [Eq. (6)], $\tilde{\eta}$ is the "rotational viscosity" that determines the orientational decay time, and μ is the cross-coupling Onsager coefficient. We have defined $\delta\tilde{Q}_{ij} \equiv (\delta Q_{ij} - \xi_1^2 \nabla^2 \delta Q_{ij} - \xi_2^2 \nabla_j \nabla_k \delta Q_{ki})$ for simplicity. The fluctuating force conjugate to the local-anisotropy production rate is found by taking a functional derivative of the standard Landau–de Gennes free energy $(\delta F/\delta Q_{ij}) = -\chi_0^{-1}\delta\tilde{Q}_{ij}$, and linearizing the resulting expression. The Landau–de Gennes free energy [14] is given by

$$F = \int d^3x \frac{1}{2}\chi_0^{-1}(Q_{ij}Q_{ji} + \xi_1^2 \nabla_i Q_{jk} \nabla_i Q_{jk} + \xi_2^2 \nabla_j Q_{jk} \nabla_i Q_{ik}) + \cdots, \tag{A3}$$

where we have omitted higher order terms that do not contribute in the linear theory. Since the contributions from the two different correlation lengths ξ_1 and ξ_2 cannot be experimentally distinguished in a conventional light-scattering experiment [20], we instead use an effective correlation length ξ, i.e., $\delta\tilde{Q}_{ij} \simeq (1-\xi^2\nabla^2)\delta Q_{ij}$. The coefficient of the second term in the expression for Φ_{ij} is necessarily positive since Q_{ij} and v_i have opposite signatures under time reversal. We have ignored fluctuations in the local pressure because we are not interested in propagating modes (sound) in the solution. Additionally, to ensure that Q_{ij} remains traceless, we only consider incompressible flow, i.e., $\nabla_i v_i = 0$. If the cross-coupling

coefficient μ is set to zero, Eq. (A2) leads to Eq. (1) and the linearized Navier-Stokes equation.

Inserting the phenomenological relations [Eq. (A2)] into the balance laws [Eq. (A1)], and taking a spatial Fourier transform $\int_{-\infty}^{\infty}\exp(i\mathbf{q}\cdot\mathbf{x})d^3x$, we obtain the resulting hydrodynamic equations,

$$\frac{\partial(\delta Q_{xy})}{\partial t} = -\frac{1}{\tau}\delta Q_{xy} + \delta\Phi_{xy}, \tag{A4}$$

$$\frac{\partial(\delta Q_{yz})}{\partial t} = -\frac{1}{\tau}\delta Q_{yz} + iq\frac{\sqrt{2}\mu}{2}\delta v_y + \delta\Phi_{yz}, \tag{A5}$$

$$\frac{\partial(\delta v_y)}{\partial t} = iq\frac{\sqrt{2}\mu}{\chi\rho}\delta Q_{yz} - \nu q^2\delta v_y + q\,\delta\Pi_{yz}/\rho, \tag{A6}$$

where $\nu=\eta/\rho$ is the kinematic viscosity. Arriving at the above equations, we have used the fact that $\mathbf{q}=-q\hat{\mathbf{z}}$ for our choice of scattering geometry. Since $\mathbf{q}$ points in the negative z direction, only gradients in the z direction survive the Fourier transform. Hence, only the coupling between δQ_{yz} and δv_y is relevant to the derivation of the autocorrelation functions, since δv_x and δv_z no longer couple to either δQ_{yz} or δQ_{xy} in the transformed Eqs. (A4)–(A6).

The full autocorrelation functions are found by taking a Laplace transform in time $\int_0^{\infty}\exp(-st)dt$ of Eqs. (A4)–(A6), where s is a frequency variable, solving the resulting set of algebraic equations, and taking an ensemble average of the product $\delta Q_{ij}^*(q,0)\delta Q_{ij}(q,s)$. With the aid of the fluctuation dissipation theorem $\langle|\delta Q_{ij}(q,0)|^2\rangle=k_BT\chi/l_0^3\equiv C$ [19], the preceding steps yield

$$\langle\delta Q_{yz}^*(q,0)\delta Q_{yz}(q,s)\rangle = C\frac{s+\nu q^2}{(s+1/\tau)(s+\nu q^2)+\mu^2q^2/\chi\rho}, \tag{A7}$$

$$\langle\delta Q_{xy}^*(q,0)\delta Q_{xy}(q,s)\rangle = C\frac{1}{s+1/\tau}. \tag{A8}$$

The above equations make the standard assumptions that there are no cross correlations between the initial configurations of the dynamic variables and the fluctuating forces.

As discussed in the body of the text, $1/\nu q^2 \ll \tau$ for all experimental values of q and temperature. Consequently we only need to consider the approximate roots of the denominator $(s+1/\tau)(s+\nu q^2)+\mu^2q^2/\chi\rho$ in Eq. (A8) to leading order in the small quantity $1/\tau\nu q^2$. With the previously discussed approximation $\eta\simeq\tilde{\eta}$, this leads to the final expression for the δQ_{yz} autocorrelation function,

$$\langle\delta Q_{yz}^*(q,0)\delta Q_{yz}(q,s)\rangle \simeq C\frac{1}{s+(1+\mu^2)/\tau}. \tag{A9}$$

Finally, the experimentally defined correlation functions given by Eq. (10) can be recovered by taking the inverse Laplace transform of Eqs. (A8) and (A9).

[1] Yu. A. Nastishin, H. Liu, S. V. Shiyanovskii, O. D. Lavrentovich, A. F. Kostko, and M. A. Anisimov, Phys. Rev. E **70**, 051706 (2004).

[2] J. E. Lydon, in *Handbook of Liquid Crystals*, edited by D. Demus, J. Goodby, G. W. Gray, H.-W. Spiess, V. Vill (Willey-VCH, New York, 1998), Vol. 2B, Chap. XVIII, p. 981.

[3] J. Lydon, Curr. Opin. Colloid Interface Sci. **3**, 458 (1998).

[4] J. Israelashvili, *Intermolecular and Surface Forces*, 2nd ed. (Academic Press, London, 1992).

[5] N. H. Hartshorne and G. D. Woodard, Mol. Cryst. Liq. Cryst. **23**, 343 (1973).

[6] M. R. Tomasik and P. J. Collings, J. Phys. Chem. B **112**, 9883 (2008).

[7] P. K. Maiti, Y. Lansac, M. A. Glaser, and N. A. Clark, Liquid Crystals **29**, 619 (2002).

[8] Yu. A. Nastishin, H. Liu, T. Schneider, V. Nazarenko, R. Vasyuta, S. V. Shiyanovskii, and O. D. Lavrentovich, Phys. Rev. E **72**, 041711 (2005).

[9] X. Ding, T. C. Stringfellow, and J. R. Robinson, J. Pharm. Sci. **93**, 1351 (2004).

[10] M. Bohorquez, C. Koch, T. Trygstad, and N. Pandit, J. Colloid Interface Sci. **216**, 34 (1999).

[11] C. Wu, T. Liu, and B. Chu, Macromolecules **30**, 4574 (1997).

[12] P. C. Hohenberg and B. I. Halperin, Rev. Mod. Phys. **49**, 435 (1977).

[13] P. M. Chaikin and T. C. Lubenski, *Principles of Condensed Matter Physics* (Cambridge University Press, Cambridge, 1995).

[14] P. G. de Gennes and J. Prost, *The Physics of Liquid Crystals* (Clarenton Press, Oxford, 1993).

[15] M. Kleman and O. D. Lavrentovich, *Soft Matter Physics: An Introduction* (Springer, New York, 2003).

[16] E. M. Lifshitz and L. P. Pitaevskii, *Physical Kinetics* (Pergamon Press, Oxford, New York, 1993).

[17] M. A. Anisimov, V. P. Voronov, A. S. Goldenstein, E. E. Gorodetskii, Y. F. Kiyachenko, and V. M. Merkulov, Sov. Phys. JETP **60**, 1134 (1984).

[18] M. A. Anisimov, *Critical Phenomena in Liquids and Liquid Crystals* (Gordon and Breach Science Publishers, New York, 1991).

[19] L. D. Landau and E. M. Lifshitz, *Statistical Physics* (Pergamon Press, Oxford, New York, 1980).

[20] T. W. Stinson and J. D. Litster, Phys. Rev. Lett. **30**, 688 (1973).

[21] L. D. Landau and E. M. Lifshitz, *Fluid Mechanics* (Pergamon Press, Oxford, New York, 1987).

[22] H. C. Andersen, R. Pecora, J. Chem. Phys. **54**, 2584 (1971).

[23] A. F. Kostko, B. H. Cipriano, O. A. Pinchuk, L. Ziserman, M. A. Anisimov, D. Danino, and S. R. Raghavan, J. Phys. Chem. B **109**, 19126 (2005).

[24] A. F. Kostko, M. A. Anisimov, and J. V. Sengers, Phys. Rev. E **76**, 021804 (2007).

[25] J. Jacob, M. A. Anisimov, J. V. Sengers, V. A. Dechabo, I. K. Yudin, and R. W. Gammon, Appl. Opt. **40**, 4160 (2001).
[26] A. F. Kostko, M. A. Anisimov, and J. V. Sengers, Phys. Rev. E **70**, 026118 (2004).
[27] M. A. Anisimov, A. F. Kostko, J. V. Sengers, and I. K. Yudin, J. Chem. Phys. **123**, 164901 (2005).
[28] I. D. Olenik, L. Spindler, M. Copic, H. Sawade, D. Kruerke, and G. Heppke, Phys. Rev. E **65**, 011705 (2001).
[29] B. J. Berne and R. Pecora, *Dynamic Light Scattering with Applications to Chemistry, Biology, and Physics* (Wiley, New York, 1976).
[30] K. Zero and R. Pecora, in *Dynamic Light Scattering. Applications of Photon Correlation Spectroscopy*, edited by R. Pecora (Plenum Press, New York, 1985).
[31] A. Yu. Val'kov, V. P. Romanov, and A. N. Shalaginov, Phys. Usp. **37**, 139 (1994).
[32] L. V. Adjemyan, L. T. Adjemyan, A. Yu. Val'kov, L. A. Zubkov, I. A. Mel'nik, and V. P. Romanov, Sov. Phys. JETP **60**, 712 (1984).
[33] P. S. Russo, in *Dynamic Light Scattering. The Method and Some Applications*, edited by W. Brown (Clarendon Press, Oxford, 1993).
[34] H. Tanaka, Y. Nakanishi, and N. Takubo, Phys. Rev. E **65**, 021802 (2002).
[35] P. A. Hassan, S. R. Raghavan, and E. W. Kaler, Langmuir **18**, 2543 (2002).
[36] D. Kivelson and R. Hallem, Mol. Phys. **38**, 1411 (1979).
[37] D. F. Calef and P. G. Wolynes, J. Chem. Phys. **72**, 535 (1980).
[38] B. Loppinet, G. Fytas, G. Petekidis, T. Sato, and G. Wegner, Eur. Phys. J. E **8**, 461 (2002).
[39] R. G. Cole, D. K. Hoffman, and G. T. Evans, J. Chem. Phys. **80**, 5365 (1984).
[40] R. G. Larson, *The Structure and Rheology of Complex Fluids* (Oxford University Press, Oxford, 1999).
[41] J. M. Ortiz de Zárate and J. V. Sengers, *Hydrodynamic Fluctuations in Fluids and Fluid Mixtures* (Elsevier, Amsterdam, 2006).
[42] M. L. Jiménez, F. Mantegazza, L. Gallazzi, G. Zanchetta, and T. Bellini, Phys. Rev. E **74**, 011707 (2006).
[43] J. Prost and P. G. de Gennes, *Simple Views on Condensed Matter* (World Scientific, Singapore, 2003), 3rd ed., p. 78.